

Antilocalization and spin-orbit coupling in hole strained GaAs/In_xGa_{1-x}As/GaAs quantum well heterostructures

G. M. Minkov and A. A. Sherstobitov

Institute of Metal Physics RAS, 620219 Ekaterinburg, Russia

A. V. Germanenko, O. E. Rut, and V. A. Larionova

Institute of Physics and Applied Mathematics, Ural State University, 620083 Ekaterinburg, Russia

B. N. Zvonkov

Physical-Technical Research Institute, University of Nizhni Novgorod, 603600 Nizhni Novgorod, Russia

Low-field magnetoresistance in *p*-type strained quantum wells is studied. It is shown that the Rashba mechanism leads to the cubic in quasimomentum spin-orbit splitting of the hole energy spectrum and the antilocalization behavior of low-field magnetoresistance is well described by the Hikami-Larkin-Nagaoka expression.

PACS numbers: 73.20.Fz, 73.61.Ey

The combination of quantum coherence and spin rotation produces a number of interesting transport properties. Numerous proposals for electronic devices that use spin-orbit coupling have appeared in last years, including gate-controlled sources and detectors of spin-polarized current.^{1,2,3} Spin-orbit coupling results in the spin splitting of the energy spectrum when an inversion symmetry is lifted. The lack of inversion symmetry of the original crystal results in the splitting of the energy spectrum, which is linear and cubic in in-plane quasimomentum, k . This splitting is described by terms known as the Dresselhaus terms.⁴ In low-dimensional systems an additional mechanism of spin splitting is caused by the asymmetry of the confining potential (so called the Rashba term⁵). In two-dimensional (2D) semiconductor systems this asymmetry arises from asymmetry of the smooth electrostatic potential in the perpendicular to the 2D plane direction, from Schottky barrier potential, from asymmetry in doping layers disposition, and composition gradient along the growth direction. It is very important that this asymmetry can be controlled by gate voltage. For electron 2D states, the Rashba term is linear in k . For hole 2D systems, the situation becomes more complicated because of four-fold degeneracy of the top-most valence band Γ_8 of the parent material. Theoretical considerations of this problem and experimental studies show that the splitting is cubic in k in this case.^{6,7,8,9}

The measurements of interference induced low-field magnetoresistance are the powerful tool for studies of the spin-splitting, spin- and phase- relaxation mechanisms. At present, there are numerous studies of *n*-type 2D systems^{2,10,11,12,13,14,15,16}, whereas the more complicated *p*-type systems are studied noticeable less^{17,18,19,20,21} (for more references see review article by Zawadzki and Pfeffer²²). As for the strained quantum well, the antilocalization and spin relaxation in 2D hole gas are practically not investigated in these systems.

In this paper, we present results of experimental study of the low-field magnetoresistance caused by spin relax-

ation in *p*-type strained GaAs/In_xGa_{1-x}As/GaAs quantum well structures. It has been found that the magnetoresistance shape is well described by the Hikami-Larkin-Nagaoka (HLN) expression²³ that means that the leading term in the spectrum splitting is cubic in quasimomentum. We show that in contrast to *n*-type systems, where such a finding implies that the Dresselhaus spin splitting mechanism is the main, the Rashba mechanism is responsible for the spin splitting of the hole energy spectrum in strained quantum wells under investigation.

The GaAs/In_xGa_{1-x}As/GaAs heterostructures were grown by metal-organic vapor phase epitaxy on semi-insulator GaAs substrate. The quantum well was biaxially compressed due to the lattice mismatch between In_xGa_{1-x}As and GaAs. Two types of heterostructures were studied. The structures of the first type, 3855, 3856, and 3857, consist of a 250 nm-thick undoped GaAs buffer layer, carbon δ -layer, a 7 nm spacer of undoped GaAs, a 8 nm In_{0.2}Ga_{0.8}As well, a 7 nm spacer of undoped GaAs, a carbon δ -layer and 200 nm cap layer of undoped GaAs (see Fig. 1). The structure of the second type, 3951, was analogous, the only difference was the wider spacer, 15 nm, and as sequence the higher mobility. The structures within the first group differ by carbon density in δ -layers. The parameters of the structures are presented in Table I. The samples were mesa etched into standard Hall bars and then an Al gate electrode was deposited by thermal evaporation onto the cap layer through a mask. Varying the gate voltage V_g from -1 V to +3 V we changed the hole density in the quantum well from $3 \times 10^{11} \text{ cm}^{-2}$ to $1 \times 10^{12} \text{ cm}^{-2}$. The analysis of the temperature dependence of the Shubnikov-de Haas oscillations showed that the hole effective mass was equal to $(0.160 \pm 0.005)m_0$ and did not depend on the hole density.

Figure 2 shows the low-field magnetoconductivity, $\Delta\sigma(B) = \rho_{xx}^{-1}(B) - \rho_{xx}^{-1}(0)$, measured at $T = 0.44 \text{ K}$ for structure 3857 as a function of a normalized magnetic field $b = B/B_{tr}$, where $B_{tr} = \hbar/(2el^2)$ with l as the mean

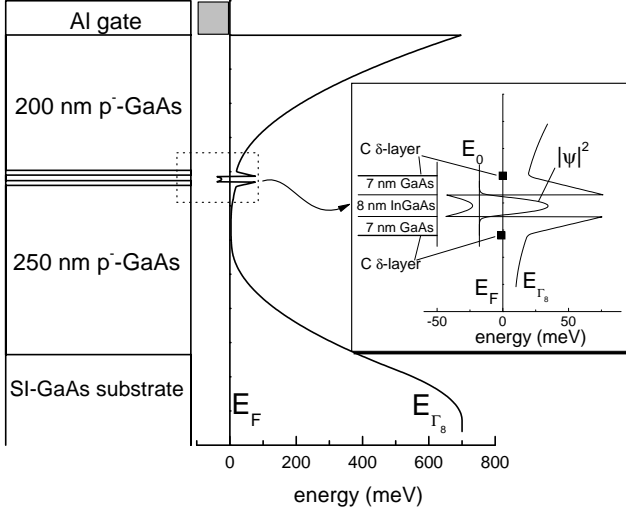


FIG. 1: The cross section of structure 3857 and its energy diagram.

free path, is presented in Fig. 2. The antilocalization maximum at $B = 0$ in the conductivity-versus-magnetic field curves decreases with lowering hole density and disappears at $V_g = 2.75$ V, when $p \simeq 3.8 \times 10^{11} \text{ cm}^{-2}$. In the structures 3951 with the higher hole mobility, the disappearance happens at $p \simeq 3 \times 10^{11} \text{ cm}^{-2}$.

Theoretically, the low-field anomalous magnetoresistance was studied in Refs.11,23,25. It was shown that when the spin splitting is cubic in k , the magnetoconductivity curve should be described by the Hikami-Larkin-Nagaoka (HLN) expression

$$\begin{aligned} \frac{\Delta\sigma(b)}{G_0} = & \psi\left(\frac{1}{2} + \frac{\tau_1}{b} \left[\frac{1}{\tau_\phi} + \frac{1}{\tau_s}\right]\right) - \ln\left(\frac{\tau_1}{b} \left[\frac{1}{\tau_\phi} + \frac{1}{\tau_s}\right]\right) \\ & + \frac{1}{2}\psi\left(\frac{1}{2} + \frac{\tau_1}{b} \left[\frac{1}{\tau_\phi} + \frac{2}{\tau_s}\right]\right) - \frac{1}{2}\ln\left(\frac{\tau_1}{b} \left[\frac{1}{\tau_\phi} + \frac{2}{\tau_s}\right]\right) \\ & - \frac{1}{2}\psi\left(\frac{1}{2} + \frac{\tau_1}{b} \frac{1}{\tau_\phi}\right) + \frac{1}{2}\ln\left(\frac{\tau_1}{b} \frac{1}{\tau_\phi}\right). \end{aligned}$$

Here, $G_0 = e^2/(2\pi^2\hbar)$, τ_ϕ and τ_s are the phase and spin relaxation times, respectively, $\psi(x)$ is the digamma function, and τ_n , $n = 1$, is the transport relaxation time

$$\frac{1}{\tau_n} = \int W(\theta)(1 - \cos n\theta)d\theta, \quad (2)$$

TABLE I: The parameters of structures investigated

Structure	$N_1 \text{ (cm}^{-2}\text{)}^a$	$N_2 \text{ (cm}^{-2}\text{)}^a$	$p \text{ (cm}^{-2}\text{)}$	$\mu \text{ (cm}^2\text{/Vs)}$
3855	4×10^{11}	3×10^{11}	4.7×10^{11}	4800
3856	8×10^{11}	6×10^{11}	7.5×10^{11}	5700
3857	1.2×10^{12}	8×10^{11}	9.5×10^{11}	8000
3951	1.2×10^{12}	8×10^{11}	5.4×10^{11}	13100

^a N_1 and N_2 are the carbon density in outer and inner δ -layers, respectively.

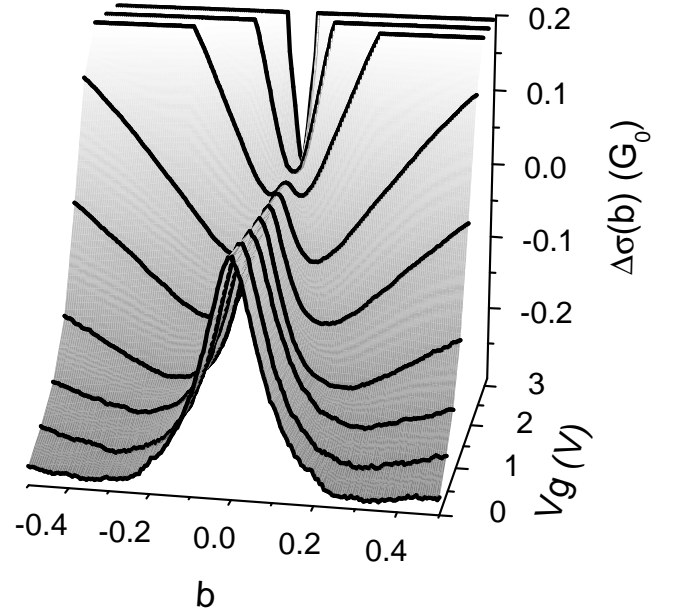


FIG. 2: The magnetoconductivity plotted against the reduced magnetic field for different gate voltages, structure 3857, $T = 0.44$ K.

where $W(\theta)$ stands for the probability of the scattering by an angle θ .

For the Dyakonov-Perel spin-relaxation mechanism,²⁴ which is dominant at low temperatures, the value of τ_s is determined by the spin-orbit splitting of the energy spectrum, $\hbar\Omega_3 \propto k^3$, as follows

$$\frac{1}{\tau_s} = 2\Omega_3^2\tau_3 \quad (3)$$

where τ_3 is defined by Eq. (2).

Taking into account both the cubic and linear terms leads to more complicated expression which was obtained (1) in Ref. 25. The following two parameters describing the spin relaxation arise in this case

$$\frac{1}{\tau'_s} = 2\Omega_1^2\tau_1 \quad (4)$$

and

$$\frac{1}{\tau_s} = 2(\Omega_1^2\tau_1 + \Omega_3^2\tau_3), \quad (5)$$

where $\hbar\Omega_1$ is the linear in k , $\hbar\Omega_1 \propto k$, spin-orbit splitting.

Comparison of the experimental data with theoretical expressions for two limiting cases, when only the cubic or linear term is taken into account, is shown in Fig. 3. To span the characteristic minima in $\Delta\sigma$ -versus- B curves, the fitting interval has been chosen as $-0.3B_{tr} < B < 0.3B_{tr}$. Strictly speaking, the boundaries of this interval do not satisfy the diffusion approximation $B \ll B_{tr}$ in which framework the formulae for

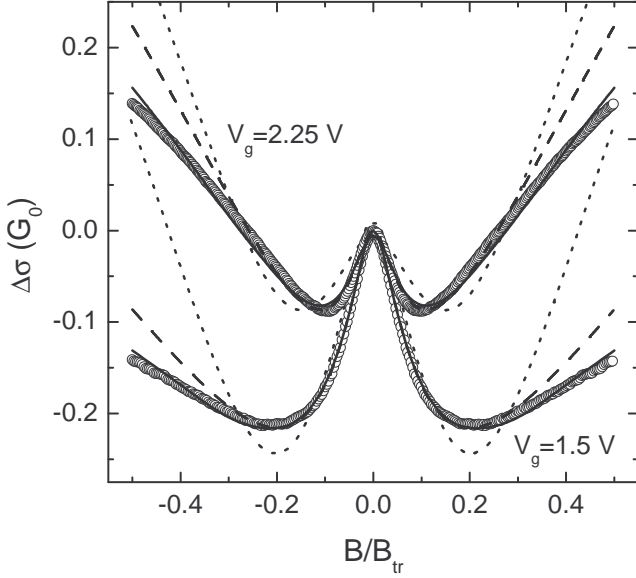


FIG. 3: The magnetoconductivity as a function of normalized magnetic field for the two gate voltages: $V_g = 1.5$ V ($p = 8 \times 10^{11}$ cm $^{-2}$, $\tau_1 = 5.4 \times 10^{-13}$ s) and $V_g = 2.25$ V ($p = 5.8 \times 10^{11}$ cm $^{-2}$, $\tau_1 = 3.9 \times 10^{-13}$ s); structure 3857, $T = 0.44$ K. Symbols are the experimental data. The dotted lines are the best fit by the expression from Ref. 25 when only the linear in k term is taken into account. Dashed lines are the best fit by the HLN expression, Eq. (1). Solid lines are the results of the simulation procedure (see Appendix A) which is valid beyond the diffusion approximation. The fit has been done within the magnetic field range $-0.3B_{tr} < B < 0.3B_{tr}$. The fitting parameters are given in Table II.

magnetoconductance^{23,25} has been derived. Nevertheless, one can see that the taking into account only the linear term does not allow us to describe satisfactorily the magnetoconductivity shape within the fitting interval while the HLN expression gives a good agreement. Beyond the diffusion regime, the HLN theory was generalized by Zduniak *et al.*¹³ However, the final expressions are very complicated and inconvenient to use in the fitting procedure. Because of this, we used the simulation approach described in our paper, Ref. 26. To take into

TABLE II: The parameters of the best fit for the data presented in Fig. 3 as obtained taking into account only the linear in k term,²⁵ only the cubic in k term in the diffusion approximation,²³ and the cubic in k term beyond the diffusion approximation (see Appendix A).

V_g (V)	Theory	τ_1/τ_ϕ	τ_1/τ_s
1.5	Ref. 25	0.020	0.178
	Ref. 23	0.016	0.051
	Appendix A	0.014	0.040
2.25	Ref. 25	0.034	0.142
	Ref. 23	0.017	0.032
	Appendix A	0.013	0.025

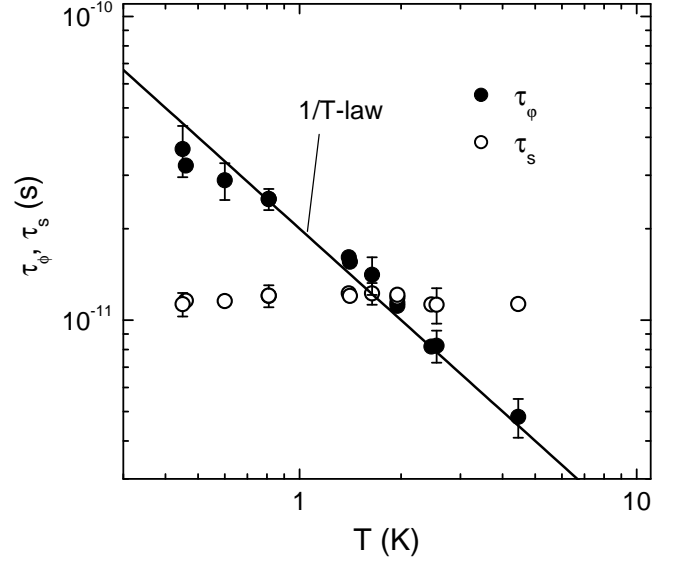


FIG. 4: The temperature dependence of the phase and spin relaxation time as obtained from the fit of the experimental data by Eq. (1) for structure 3857 at $V_g = 1.5$ V. Solid line is the T^{-1} -law.

account the spin-relaxation processes, Eq. (20) from this paper was modified as described in Appendix A (details will be published elsewhere). As Fig. 3 illustrates, with the use of Eq. (A1) we obtain a nice coincidence of calculated and measured curves over the whole magnetic field range. Although the theory beyond the diffusion approximation describes the magnetoresistance curve better, the fitting parameters τ_1/τ_ϕ and τ_1/τ_s are found to be close to those obtained with the help of Eq. (1) (see Table II). Therefore, it seems natural to analyze the experimental results with the use of the more simple HLN expression.

Further indication, that just the cubic in k splitting is responsible for the spin relaxation, is reasonable behavior of the fitting parameters obtained from Eq. (1) with the temperature change. As seen from Fig. 4 the parameter τ_ϕ exhibits the behavior close to T^{-1} -law that corresponds to the phase relaxation caused by inelasticity of electron-electron interaction.²⁷ The parameter τ_s is temperature independent as should be for degenerated electron gas. Such analysis has been carried out for all the structures investigated and the results are collected in Fig. 5 as a plot of the spin relaxation time τ_s against the hole density controlled by the gate voltage.

For the first sight the fact that the magnetoconductance curves are well described by the HLN expression means that the Dresselhaus cubic term gives the main contribution to the spin splitting in the structure investigated. Whether or not it is so, one can understand analyzing the hole density dependence of spin-orbital splitting, $\hbar\Omega_3(p)$. For the Dresselhaus mechanism, the splitting should be proportional to $p^{3/2}$ because $\Omega_3 = \gamma k^3/4$, where γ is constant depending only on the band parameters of the parent material (see Appendix A in Ref. 11

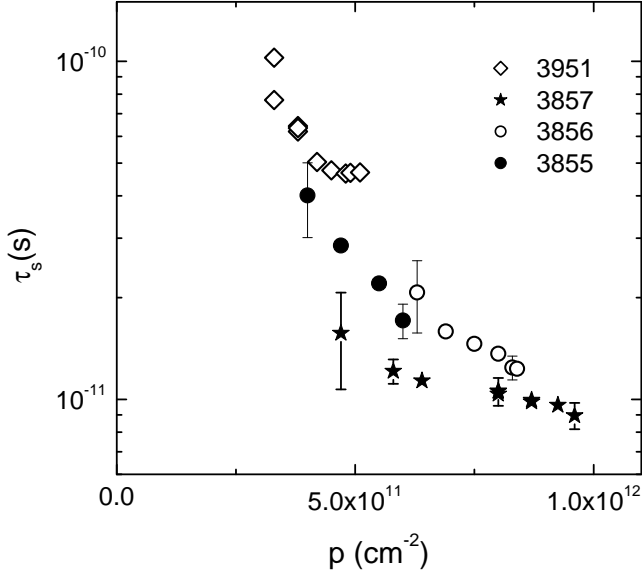


FIG. 5: The spin relaxation time as a function of hole density controlled by the gate voltage for all structures investigated, $T = 0.44$ K.

for details). Experimentally, the value of spin-orbit splitting $\hbar\Omega_3$ can be found from Eq. (3) using τ_s obtained above and τ_3 . How the quantity τ_3 has been obtained is considered below.

As seen from Eq. (2) the relaxation time τ_3 is determined by the scattering anisotropy via the function $W(\theta)$. Just the same function determines the relationship between the quantum and transport relaxation times, τ_0 and τ_1 , respectively. Therefore, we estimate τ_3 using the experimental value for τ_0

$$\tau_3 = \tau_0 \int W(\theta) d\theta / \int W(\theta) (1 - \cos 3\theta) d\theta, \quad (6)$$

and conceiving the physically reasonable angle dependence for $W(\theta)$ so that the ratio

$$K_{01} = \int W(\theta) (1 - \cos \theta) d\theta / \int W(\theta) d\theta, \quad (7)$$

to be equal to the experimental quantity τ_0/τ_1 . The value of τ_0 has been obtained from the analysis of the magnetic field dependence of the amplitude of the Shubnikov-de Haas oscillations, while τ_1 has been found from the mobility value, $\tau_1 = \mu m/e$. The experimental hole density dependences of τ_0 and τ_1 , presented in Fig. 6, show that the scattering is really anisotropic in all the structures and the τ_0 to τ_1 ratio lies in the interval from 0.2 to 0.5. This seemingly points to the fact that the scattering is mainly determined by ionized impurities and $W(\theta)$ can be chosen in the form obtained, e.g., in Ref. 29. However, our estimation shows that the electron mobility in this case should be one-two order of magnitude higher than that observed experimentally. We suppose that the

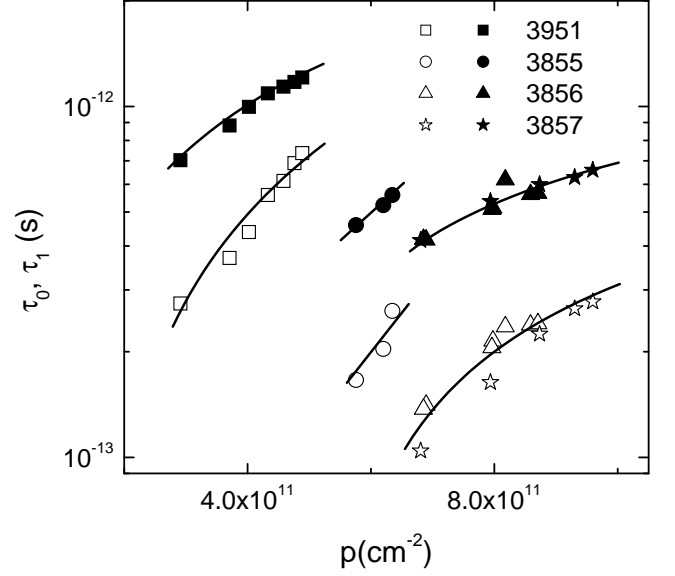


FIG. 6: The hole density dependence of τ_0 (open symbols) and τ_1 (solid symbols). Solid lines are provided as a guide for the eye.

roughness of the quantum well interfaces restricts the mobility in our structures. This mechanism is theoretically studied in Ref. 30, where the explicit form for $W(\theta)$ is derived and it is shown that the scattering anisotropy strongly depends on the parameter Λ characterizing the fluctuations of the quantum well width due to interfaces roughness. Using the form for $W(\theta)$ from this paper we have chosen such a value of parameter Λ which satisfies the equality between the experimental value of τ_0/τ_1 and the calculated from Eq. (7) value of K_{01} . Then, with this Λ -value we have calculated τ_3 to τ_0 ratio. Doing so we have found that $\tau_3 = (0.7 \dots 0.8)\tau_0$ when K_{01} lies within actual for our case range, $K_{01} = 0.2 \dots 0.5$. Note, the close results, $\tau_3 \simeq \tau_0$, are obtained if one uses $W(\theta)$ corresponding to scattering by remote ionized impurities.²⁹

Finally, we arrive the key figure of the paper, Fig. 7, where the value of spin splitting $\hbar\Omega_3 = \hbar/\sqrt{2\tau_3\tau_s}$ is plotted as a function of the hole density. One can see that (i) we do not observe the characteristic for the cubic in k spin-orbit splitting $p^{3/2}$ -dependence and (ii) different structures demonstrate significantly different value of the splitting for a given hole density. Both these facts unambiguously show that no the Dresselhaus mechanism is responsible for the cubic in k spin-orbit splitting of the hole spectrum.

Let us now discuss specific features of the Rashba effect for holes in strained quantum well heterostructures. In general, this effect in hole 2D systems is considered in Refs. 6,7,8,9. Below we write out only the main expressions which help us to describe the experimental results presented quantitatively. We restrict our consideration by the case when only three hole bands are taken into account. They are the heavy- and light-hole Γ_8 bands

and split off by spin-orbit interaction Γ_7 hole band. In this case, the energy spectrum is described by the 6×6 Luttinger-Kohn Hamiltonian³¹ which includes the terms responsible for the strain.³² As shown in Ref. 33, the 6×6 Hamiltonian can be decoupled into two independent 3×3 matrices of the form

$$H = \begin{pmatrix} A_+ & C \mp iB & \sqrt{2} \pm iB/\sqrt{2} \\ C \pm iB & A_- & F \mp i\sqrt{3/2}B \\ \sqrt{2} \mp iB/\sqrt{2} & F \pm i\sqrt{3/2}B & D \end{pmatrix} \quad (8)$$

where

$$\begin{aligned} A_{\pm} &= -(\gamma_1 \mp 2\gamma_2)k_z^2 - (\gamma_1 \pm \gamma_2)k^2 + E_{\Gamma_8}(z) + V(z) \pm S \\ B &= 2\sqrt{3}\gamma_3kk_z \\ C &= \sqrt{3}k^2(\gamma_2^2 \cos^2 2\theta + \gamma_3^2 \sin^2 2\theta)^{1/2} \\ D &= -\gamma_1(k_z^2 + k^2) + E_{\Gamma_7}(z) + V(z) \\ F &= 2\gamma_2(\sqrt{2}k_z^2 - k^2/\sqrt{2}). \end{aligned}$$

Here, γ_i stand for $\hbar^2\gamma_i^L/(2m_0)$, where γ_i^L are the Luttinger parameters, k_z is the wave vector along the [001] growth direction, $k^2 = k_x^2 + k_y^2$, θ is the angle between the in-plane wave vector and the [100] direction, $V(z)$ is the macroscopic electric potential in the heterostructure, E_{Γ_8} and E_{Γ_7} are the energies of edges of corresponding bands, and

$$S = b \left(\frac{\sigma + 1}{\sigma - 1} \right) \frac{\Delta a}{a} \quad (9)$$

is the splitting of the Γ_8 band due to strain caused by the lattice mismatch between GaAs and $\text{In}_x\text{Ga}_{1-x}\text{As}$. In Eq. (9), b stands for the axial deformation potential of the valence band, σ is the Poisson's ratio, Δa is the lattice mismatch between materials of the quantum well and barrier, and a is the lattice constant of the quantum well material. Let us estimate characteristic energies for the case of GaAs/ $\text{In}_{0.2}\text{Ga}_{0.8}\text{As}$ heterostructure. The value of $\Delta a/a$ is about 1.4 %, σ is approximately equal to 1/3, b is about -1.7 eV so that the value of strain induced splitting $2|S|$ is approximately equal to 90 meV. This value is five-times greater than the Fermi energy in our case. We find the Rashba splitting of the hole energy spectrum using the ratio $E_F/(2S)$ as a small parameter. The band parameters γ_i and $\Delta = E_{\Gamma_7} - E_{\Gamma_8}$ are supposed independent of z -coordinate. Then, in isotropic approximation, $\gamma_2 = \gamma_3 = \gamma$, the energy spectrum of the upper split off band for our case can be written as follows

$$E^{\pm} \simeq E \pm \hbar\Omega_3 \quad (10)$$

with

$$\begin{aligned} \hbar\Omega_3 &= 6\gamma^2k^3 \int dz |\psi|^2 \frac{d}{dz} \left[\frac{1}{E - E_{\Gamma_8}(z) - S - V(z)} \right. \\ &\quad \left. - \frac{1}{E - E_{\Gamma_8}(z) - \Delta - V(z)} \right], \end{aligned} \quad (11)$$

where ψ and E are solutions of the Schrödinger equation

$$A_+\psi = E\psi. \quad (12)$$

It is clearly seen from Eq. (11), that the Rashba splitting for all 2D subbands formed from the upper hole band is cubic in k in contrast to the electron energy spectrum where it is linear in k .

Now we are in position to compare the experimental $\hbar\Omega_3$ -versus- p dependences with those calculated from Eqs. (11), (12). To find the electric potential $V(z)$, the Schrödinger equation has been self-consistently solved with the Poisson equation. We have used the parameters γ_i^L for $\text{In}_{0.2}\text{Ga}_{0.8}\text{As}$ and the value of band offset $\delta E_v = E_{\Gamma_8}(\text{GaAs}) - E_{\Gamma_8}(\text{In}_{0.2}\text{Ga}_{0.8}\text{As})$, which are obtained by the linear interpolation from the values of GaAs and InAs: $\gamma_1^L = -9.5$, $\gamma_2^L = -3.5$, $\delta E_v = 75$ meV, $\Delta = 0.35$ eV (the signs of the Luttinger parameters correspond to the increasing of energy into the valence band). As an example, the energy profile and the wave function for structure 3857, $V_g = 0$, is shown in Fig. 1. To describe the experimental Ω_3 -versus- p dependence for each structure, the parameter S has been used as a fitting one. One can see from Fig. 7 that we are able to describe well the experimental results obtained for different samples in our model only slightly varying the S -value from the one to other structure. The different value of strain induced splitting for different samples seems to be natural. It can result, for instance, from deviation of In-content from its nominal value. As for the value of the strain induced splitting, $2|S| \simeq 75 - 90$ meV, it corresponds to the lattice mismatch and In-content laying within the intervals (1.2 – 1.4)% and (17 – 20)%, respectively. Let us direct attention to the interesting detail. The $\hbar\Omega_3$ -versus- p dependence exhibits the corresponding to Eq. (11) behavior, $\hbar\Omega_3 \propto p^{3/2}$, only at low hole density, $p < 2 \times 10^{11} \text{ cm}^{-2}$. At higher hole density this dependence has a maximum and sign change (not shown in figure). This feature is caused by the fact that the hole density is varied by means of variation of the gate voltage. Applying the gate voltage we change not only the value of the Fermi quasimomentum but the energy profile of the quantum well as well. In this case the integral in Eq. (11) is not constant any more and gives additional p -dependence in Ω_3 . Vanishing of spin-orbit splitting at some hole density means that the quantum well in this point becomes effectively symmetric. We realize that the approximations of large strain induced splitting and z -independence of γ_i parameters made above are crude enough. Moreover, the well boundaries can be smooth and different, and the In-content can vary across the quantum well. These factors being taken into account could in principle change the value of S obtained from the fit. However, this should not change our interpretation in the large.

In summary, we have shown that the Rashba mechanism results in the cubic in k spin-orbit splitting of the hole energy spectrum in strained heterostructures. The

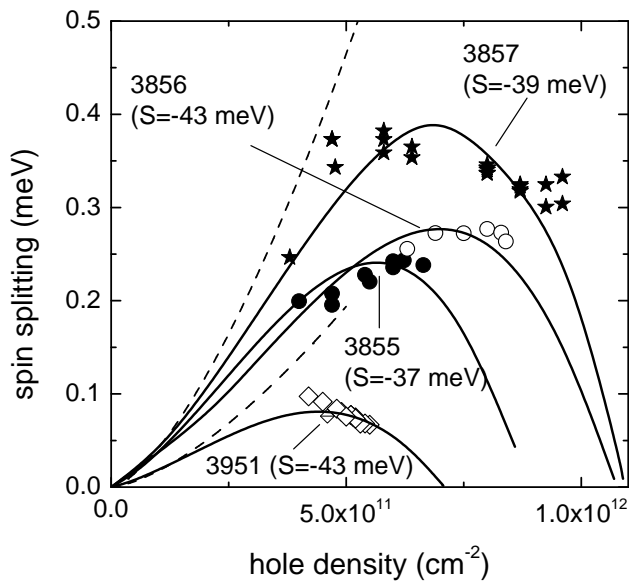


FIG. 7: The hole density dependence of the spin-orbital splitting for different samples. Symbols are the experimental data obtained as $\hbar\Omega_3 = \hbar/\sqrt{2\tau_3\tau_s}$, solid lines are calculation results (see text), dashed lines show $p^{3/2}$ -law for structures 3856 and 3951. In brackets, the values of the fitting parameter S for each structure are shown.

magnetoresistance curve in this case is well described by the HLN-expression, that allows us to find the spin splitting as a function of the hole density. We have found that these dependence is nonmonotonic at relatively high hole density due to sensitivity of quantum well profile to the gate voltage.

This work was supported in part by the RFBR (Grants 01-02-16441, 03-02-16150 and 04-02-16626), the CRDF (Grants EK-005-X1 and Y1-P-05-11), the INTAS (Grant 1B290) and the Russian Program *Physics of Solid State Nanostructures*.

APPENDIX A: NUMERICAL SIMULATION OF ANTILOCALIZATION

The weak localization phenomenon for spin-less particle using the numerical simulation of a particle motion over the plane with randomly distributed scatterers is studied both within and beyond diffusion regime in Ref. 26. It has been shown that obtaining from the simulation procedure the parameters of closed paths, one can calculate the quantum interference correction to the conductivity and its magnetic field dependence (see Eq. (20) in the paper cited). Taking into account the spin relaxation processes leads to the following expression for the interference quantum correction (in more detail this generalization will be considered elsewhere)²⁸

$$\delta\sigma(b) = -\frac{2\pi G_0}{I_s d} \sum_i \cos(bS_i) \exp(-l_i\gamma) \times \left[-\frac{1}{2} + \exp(-l_i\gamma_s) + \frac{1}{2} \exp(-2l_i\gamma_s) \right], \quad (A1)$$

where I_s is the total number of paths, d is the diameter of the area from which the particle starts to walk and in which it returns, l_i and S_i are the length and algebraic area of i -th closed path, γ and γ_s are the phenomenological parameters describing the phase and spin relaxation and corresponding in real systems to ratios τ_1/τ_ϕ and τ_1/τ_s , respectively, the lengths and areas in this expression are measured in units of mean free path and squared mean free path, respectively, and summation runs over all closed paths. In order to treat the experimental results presented in this paper, we have firstly collected the parameters of closed paths l_i and S_i simulating the motion of particle as described in Ref. 26, and, then, we have used Eq. (A1) to fit the experimental curves with γ and γ_s as the fitting parameters.

- ¹ Y. Ohno, D. K. Young, B. Beschoten, F. Matsukura, H. Ohno, and D. D. Awschalom, *Nature* **402**, 790 (1999).
- ² X. P. Wang, P. Wasilopoulos, and F. M. Peeters, *Phys. Rev. B* **65**, 165217 (2002).
- ³ T. Koga, J. Nitta, H. Takayanagi, and S. Datta, *Phys. Rev. Lett.* **88**, 126601 (2002).
- ⁴ G. Dresselhaus, *Phys. Rev.* **100**, 580 (1955).
- ⁵ Y. A. Bychkov and E. I. Rashba, *J. Phys. C* **17**, 6039 (1984).
- ⁶ L. G. Gerchikov and A. V. Subashiev, *Fiz. Tech. Poluprov.* **26**, 131 (1992) [*Sov. Phys. Semicond.* **26**, 73 (1992)].
- ⁷ R. Winkler, *Phys. Rev. B* **62**, 4245 (2000).
- ⁸ R. Winkler, H. Noh, E. Tutuc, and M. Shayegan, *Physica E* **12**, 428 (2002).
- ⁹ W. Xu and L. B. Lin, *J. Phys.: Condens. Matter* **16**, 1777 (2004).
- ¹⁰ G. L. Chen, J. Han, T. T. Huang, S. Datta, and

- D. B. Janes, *Phys. Rev. B* **47**, 4084 (1993).
- ¹¹ W. Knap, C. Skierbiszewski, A. Zduniak, E. Litwin-Staszewska, D. Bertho, F. Kobbi, J. L. Robert, G. E. Pikus, F. G. Pikus, S. V. Iordanskii, V. Mosser, K. Zekentes, and Yu. B. Lyanda-Geller, *Phys. Rev. B* **53**, 3912 (1996).
- ¹² W. Knap, A. Zduniak, L. H. Dmowski, S. Contreras, and M. I. Dyakonov, *Phys. Stat. Sol. (b)* **198**, 267 (1996).
- ¹³ A. Zduniak, M. I. Dyakonov, and W. Knap, *Phys. Rev. B* **56**, 1996 (1997).
- ¹⁴ T. Hassenkam, S. Pedersen, K. Baklanov, A. Kristensen, C. B. Sorensen, P. E. Lindelof, F. G. Pikus, and G. E. Pikus, *Phys. Rev. B* **55**, 9298 (1997).
- ¹⁵ J. B. Miller, D. M. Zumbuhl, C. M. Marcus, Y. B. Lyanda-Geller, D. Goldhaber-Gordon, K. Campman, and A. C. Gossard, *Phys. Rev. Lett.* **90**, 076807 (2003).
- ¹⁶ S. A. Studenikin, P. T. Coleridge, N. Ahmed, P. J. Poole,

- and A. Sachrajda, Phys. Rev. B **68**, 035317 (2003).
- ¹⁷ Ch. Schierholz, R. Kursten, G. Meier, T. Matsuyama, U. Merkt, Phys. Stat. Solidi (b) **233**, 436 (2002).
 - ¹⁸ S. J. Papadakis, E. P. De Poortere, H. C. Manoharan, J. B. Yau, M. Shayegan, and S. A. Lyon, Phys. Rev. B **65**, 245312 (2002).
 - ¹⁹ S. Pedersen, C. B. Sorensen, A. Kristensen, P. E. Lindelof, L. E. Golub, and N. S. Averkiev, Phys. Rev. B **60**, 4880 (1999).
 - ²⁰ L. E. Golub and S. Pedersen, Phys. Rev. B **65**, 245311 (2002).
 - ²¹ Y. Y. Proskuryakov, A. K. Savchenko, S. S. Safonov, M. Pepper, M. Y. Simmons, and D. A. Ritchie, Phys. Rev. Lett. **89**, 076406 (2002).
 - ²² W. Zawadzki and P. Pfeffer, Semicond. Sci. Technol. **19**, R1 (2004).
 - ²³ S. Hikami, A. Larkin, and Y. Nagaoka, Prog. Theor. Phys. **63**, 707 (1980).
 - ²⁴ M. I. Dyakonov and V. I. Perel, Zh. Exsp. Teor. Fiz. **60**, 1954 (1971) [Sov. Phys. JETP **33**, 1053 (1971)].
 - ²⁵ S. V. Iordanskii, Yu. B. Lyanda-Geller, and G. E. Pikus, Pis'ma Zh. Eksp. Teor. Fiz. **60**, 199 (1994) [JETP Lett. **60**, 206 (1994)].
 - ²⁶ G. M. Minkov, A. V. Germanenko, V. A. Larionova, S. A. Negashev, and I. V. Gornyi, Phys. Rev. B **61**, 13164 (2000).
 - ²⁷ B. L. Altshuler, A. G. Aronov, and D. E. Khmel'nitsky, J. Phys. C **15**, 7367 (1982).
 - ²⁸ I. V. Gornyi, private communication.
 - ²⁹ J. Lee, H. N. Spector, and V. K. Arora, J. Appl. Phys. **54**, 6995 (1983).
 - ³⁰ D. Zanato, S. Gokden, N. Balkan, B. K. Ridley, and W. J. Schaff Semicond. Sci. Technol. **19**, 427 (2004).
 - ³¹ J. M. Luttinger and W. Kohn, Phys. Rev. **97**, 869 (1955); J. M. Luttinger, Phys. Rev. **102**, 1030 (1956).
 - ³² G. E. Bir and G. L. Pikus, Symmetry and strain induced effects in semiconductors (Chichester:Wiley, 1974).
 - ³³ D. A. Broido and L. J. Sham, Phys. Rev. B **31**, 888 (1985).